Supporting Information

Activation of the PPARγ/NF-κB pathway by A-MPDA@Fe_3O_4@PVP via scavenging reactive oxygen species to alleviate hepatic ischemia-reperfusion injury

Dong Mo,[af] Wei Cui,[a] Linxin Chen,[a] Juanjuan Meng,[a] Yuting Sun,[g] Kaiyong Cai,[d] Jixi Zhang,*[d] Jianrong Zhang,*[c] Kui Wang *[de], and Xiaohe Luo *[ab]

[a] Department of Central Laboratory, Chongqing University Three Gorges Hospital, School of Medicine, Chongqing University, Chongqing, 40400, China.
[b] Department of Laboratory Medicine, Chongqing University Three Gorges Hospital, School of Medicine, Chongqing University, Chongqing, 40400, China.
[c] Department of Cardiovascular Surgery, Chongqing University Three Gorges Hospital, School of Medicine, Chongqing University, Chongqing, 40400, China.
[d] Key Laboratory of Biorheological Science and Technology, Ministry of Education, College of Bioengineering, Chongqing University, No. 174 Shazheng Road, Chongqing 400044, China.
[e] Department of Pharmacy, The Second Affiliated Hospital of Army Medical University, Chongqing 400037, China.
[f] State Key Laboratory of Biotherapy and Cancer Center, West China Hospital, West China Medical School, Sichuan University, Collaborative Innovation Center of Biotherapy, Chengdu, 610041, China.
[g] College of Biosystems Engineering and Food Science, Zhejiang University, Hangzhou, 310058, China.

* Corresponding authors:
E-mail: jixizhang@cqu.edu.cn(J. Zhang)
E-mail: jianrongzhang@cqu.edu.cn (J. Zhang);
E-mail: kuiwang@cqu.edu.cn (K. Wang);
E-mail: xiaoheluo@cqu.edu.cn (X. Luo).

Characterization

Transmission electron microscopy (TEM) images were performed on a JEM 2010 (JEOL, Japan) instrument at 200 kV acceleration to investigate the size, morphology and integrity of NPs. Samples were dried on carbon-coated Cu grids before characterization. The bulk and surface chemical compositions of samples were analyzed with high-angle annular dark-field imaging, scanning transmission electron microscopy (HAADF-STEM) and elemental mapping images using a JEM-6700F instrument (JEOL, Japan). Powder X-ray diffraction (XRD) measurements were obtained using a Bruker D8 (Germany) Advance X-Ray powder diffractometer (40 kV, 40 mA, CuKα1 radiation of λ = 1.54059 Å) with a scan speed of 2°/min and a step size of 0.02°. Nitrogen sorption isotherms were measured through an ASAP 2010 analyzer (Micrometrics, USA). XPS analysis was determined using an Axis Ultra spectrometer (Kratos, UK) with Al Ka excitation radiation at ca. 5×10^{-9} Pa. Fourier transform infrared (FTIR) spectra were recorded on a Spectrum 100 infrared spectrophotometer (PerkinElmer, USA) at a test range of 400-4,000 cm^{-1} with KBr pellet. UV-vis absorption was recorded on a UV-Vis spectrofluorometer (NanoDrop One, Thermo). Fluorescence spectra were recorded on a fluorescence spectrophotometer (RF-6000, Shimadzu, Japan) using a xenon lamp as an excitation source.

Table S1 the antibodies used in the present study.

Antibody name	Dilution ratio	kD	Source	Brand	Catalog No.
β-actin	1:1000	41.6	Mouse	ZSGB-BIO	TA-09
Caspase-3	1:1000	35/19/17	Rabbit	Cell Signaling Technology	14220
Bax	1:500	23	Mouse	SANTA CRUZ BIOTECHNOLOGY	sc-7480
Bcl-2	1:1000	26	Rabbit	abcam	ab59348
TNF-α	1:500	17/26	Mouse	SANTA CRUZ BIOTECHNOLOGY	sc-52746
IL-6	1:500	21	Mouse	SANTA CRUZ BIOTECHNOLOGY	sc-32296
IL-1β	1:1000	31	Mouse	Cell Signaling Technology	12242S
PPARγ	1:1000	57	Rabbit	Cell Signaling Technology	2435S
NF-κB	1:1000	61	Rabbit	BEIJING BIOSYNTHESIS BIOTECHNOLOGY	bs-0465R
p-NF-κB	1:1000	65	Rabbit	Cell Signaling Technology	3033S
I-κB-α	1:1000	39	Rabbit	Cell Signaling Technology	4812S
p-I-κB-α	1:1000	40	Mouse	Cell Signaling Technology	9246S
F4/80	1:1000	65-250	Rabbit	Cell Signaling Technology	70076S

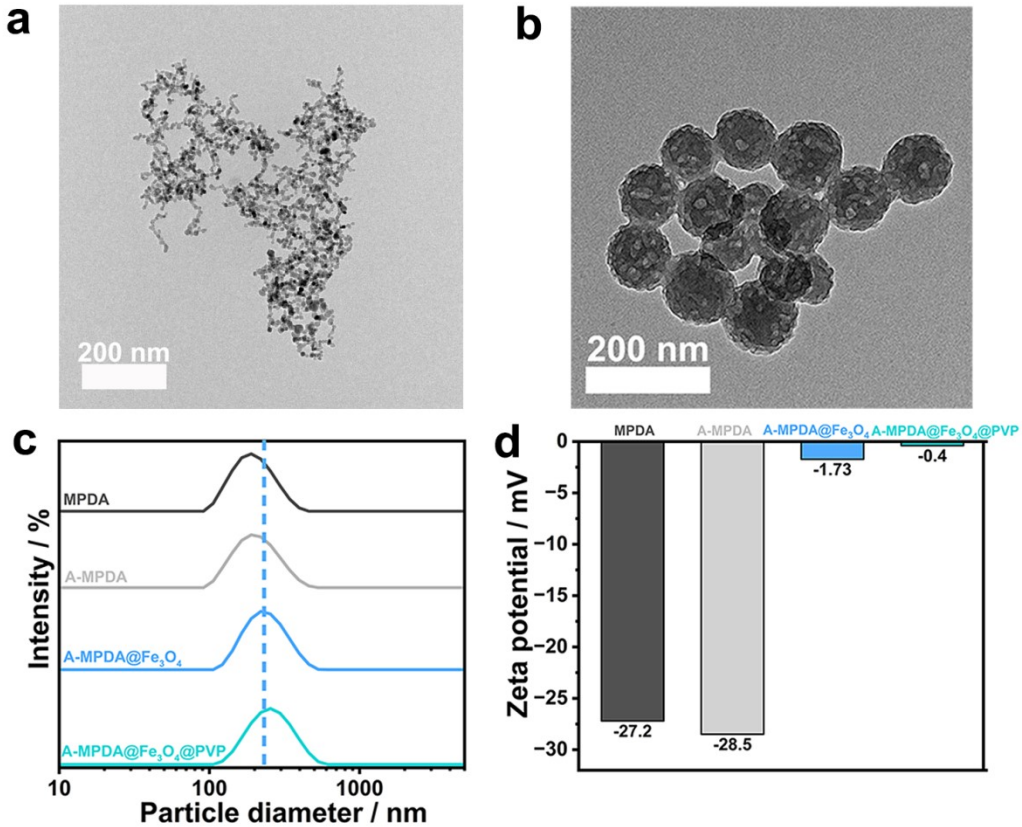

Fig. S1. TEM image of Fe_3O_4 (a) and MPDA NPs (b), DLS size distribution (c) and Zeta potential (d) of MPDA, A-MPDA, A-MPDA@Fe_3O_4, and A-MPDA@Fe_3O_4@PVP NPs in water.

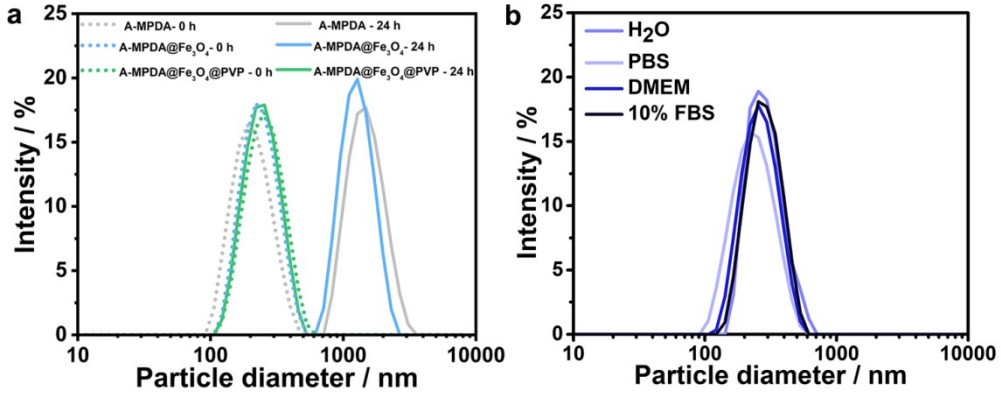

Fig. S2. (a) DLS size distribution of A-MPDA, A-MPDA@Fe_3O_4 and A-MPDA@Fe_3O_4@PVP NPs in DMEM for 0 h and 24 h. (b) DLS size distribution of A-MPDA@Fe_3O_4@PVP NPs in different dispersing solvents for 24 h.

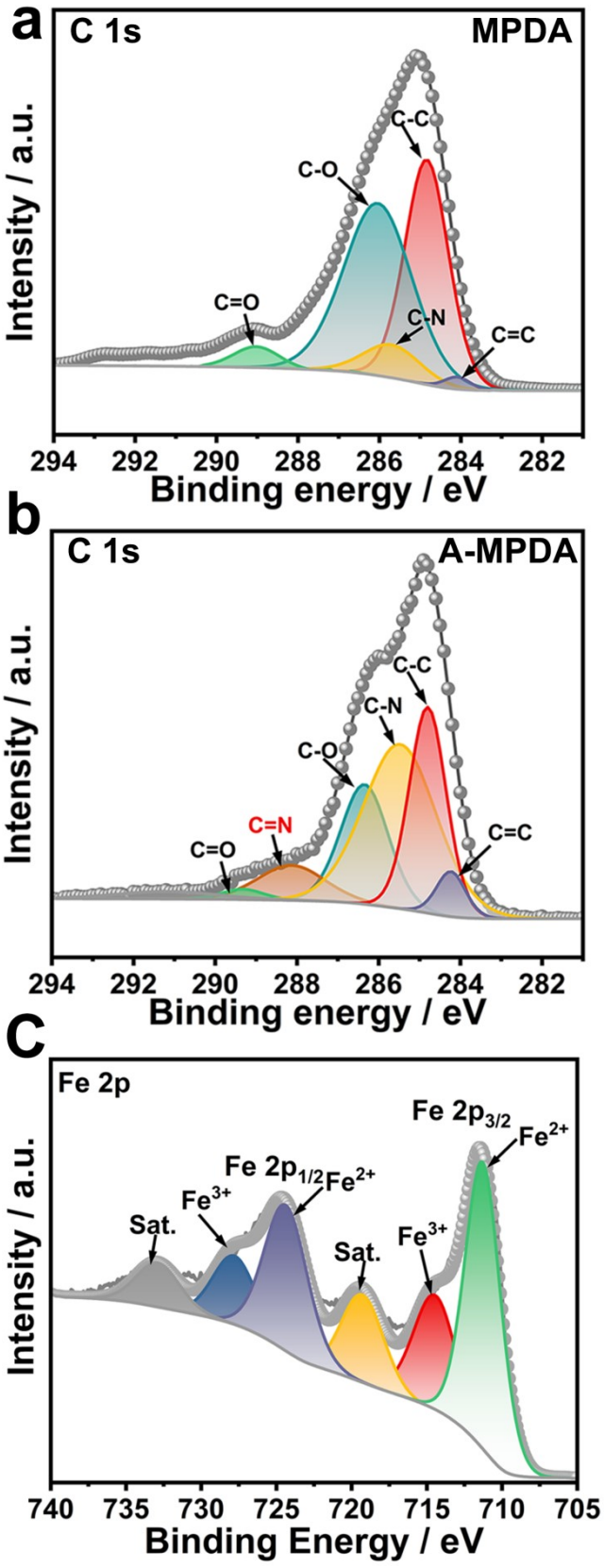

Fig. S3. High-resolution X-ray photoelectron spectra of C1s in MPDA (a) and A-MPDA NPs (b); (c) High-resolution XPS spectra of Fe 2p in A-MPDA@Fe_3O_4@PVP.

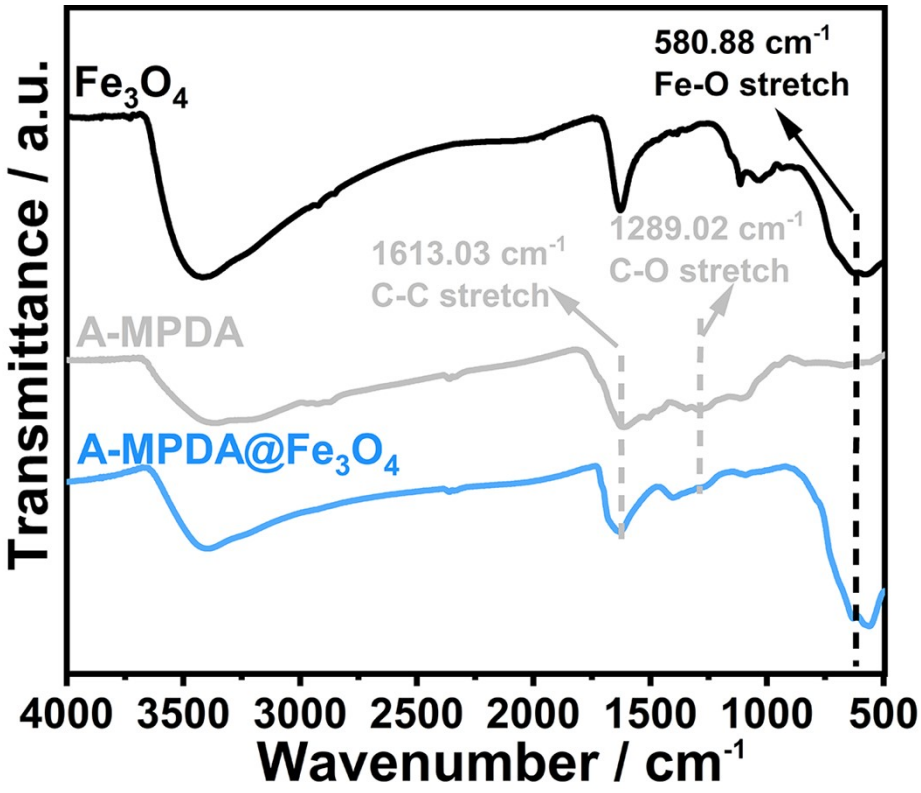

Fig. S4. Fourier transform infrared spectroscopy (FT-IR) of Fe_3O_4, A-MPDA, and A-MPDA@Fe_3O_4 NPs.

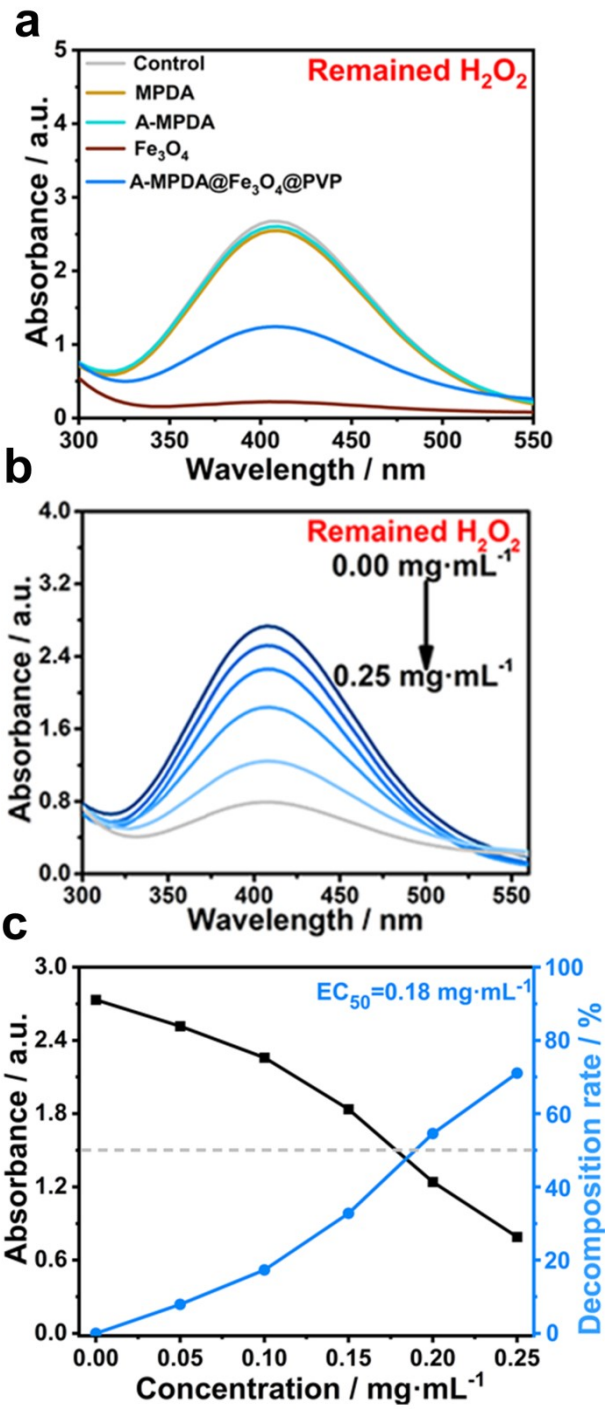

Fig. S5. (a) scavenging efficiencies of H_2O_2 with MPDA, A-MPDA, Fe_3O_4 and A-MPDA@Fe_3O_4@PVP NPs; (b) scavenging efficiencies of H_2O_2 exposed to different concentrations of A-MPDA@Fe_3O_4@PVP NPs, respectively, and the corresponding absorbance of each system and decomposition rate of A-MPDA@Fe_3O_4@PVP NPs toward H_2O_2 (c).

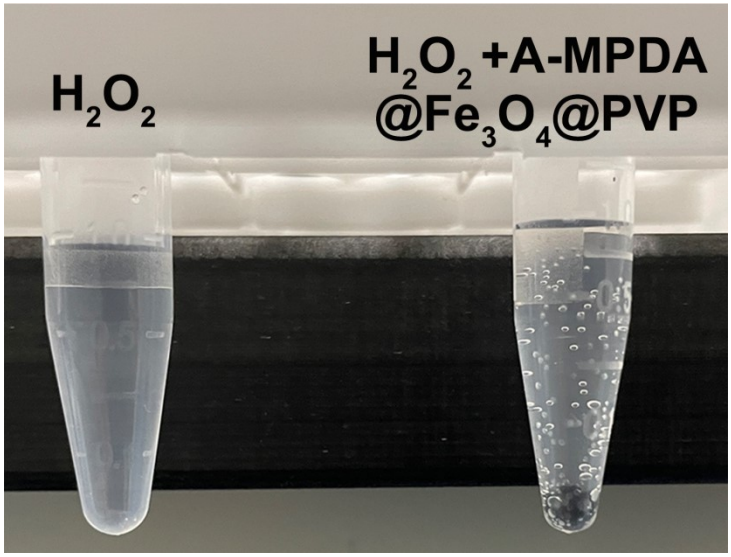

Fig. S6. O_2 bubbles observation of A-MPDA@Fe_3O_4@PVP NPs (2 mg·mL^{-1}) solution after addition of 200 mM H_2O_2.

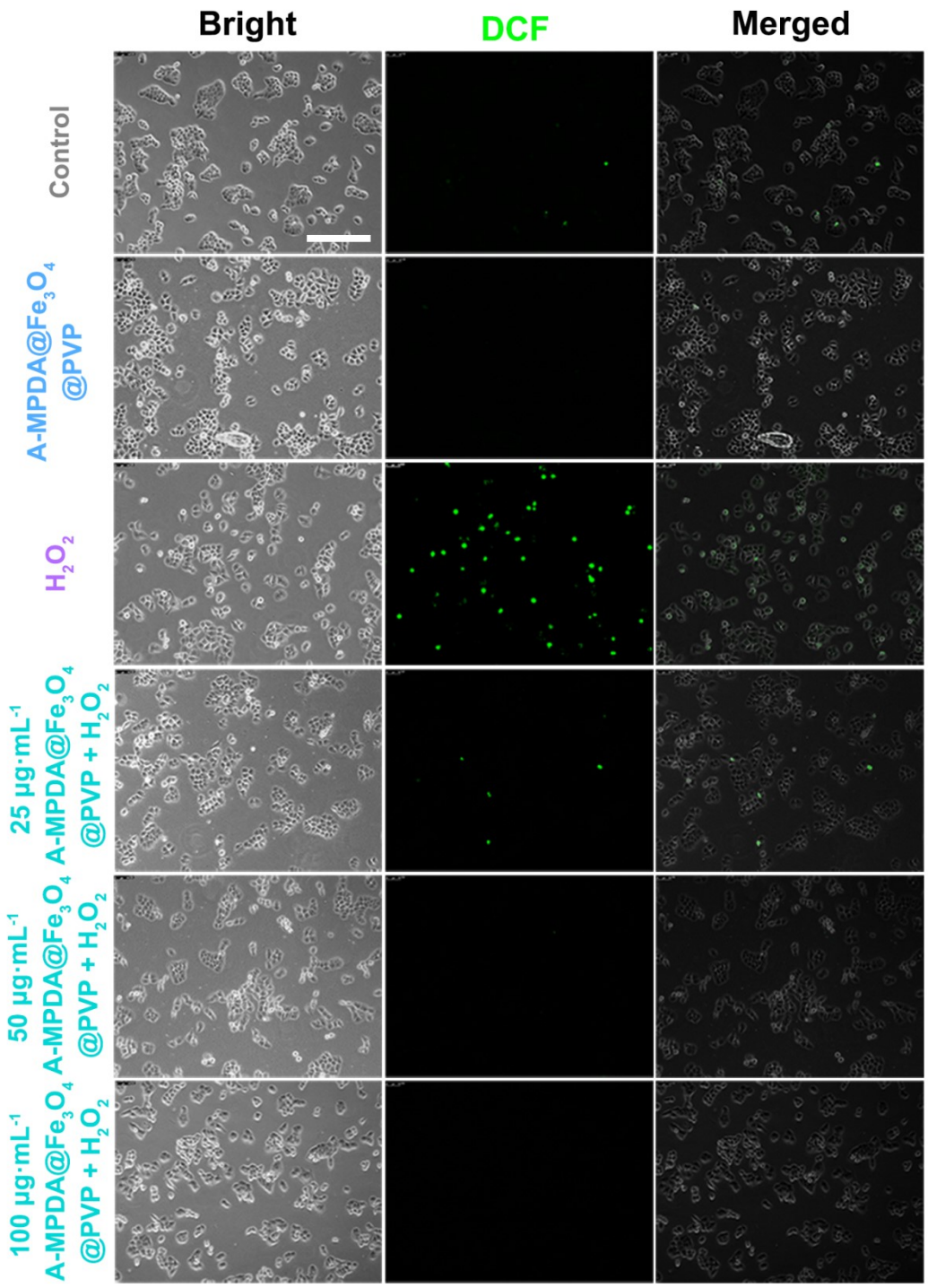

Fig. S7. Representative intracellular ROS staining of untreated and different concentration of A-MPDA@Fe_3O_4@PVP NPs-treated L02 cells with H_2O_2 treatment (200 μM). Scale bar: 300 μm.

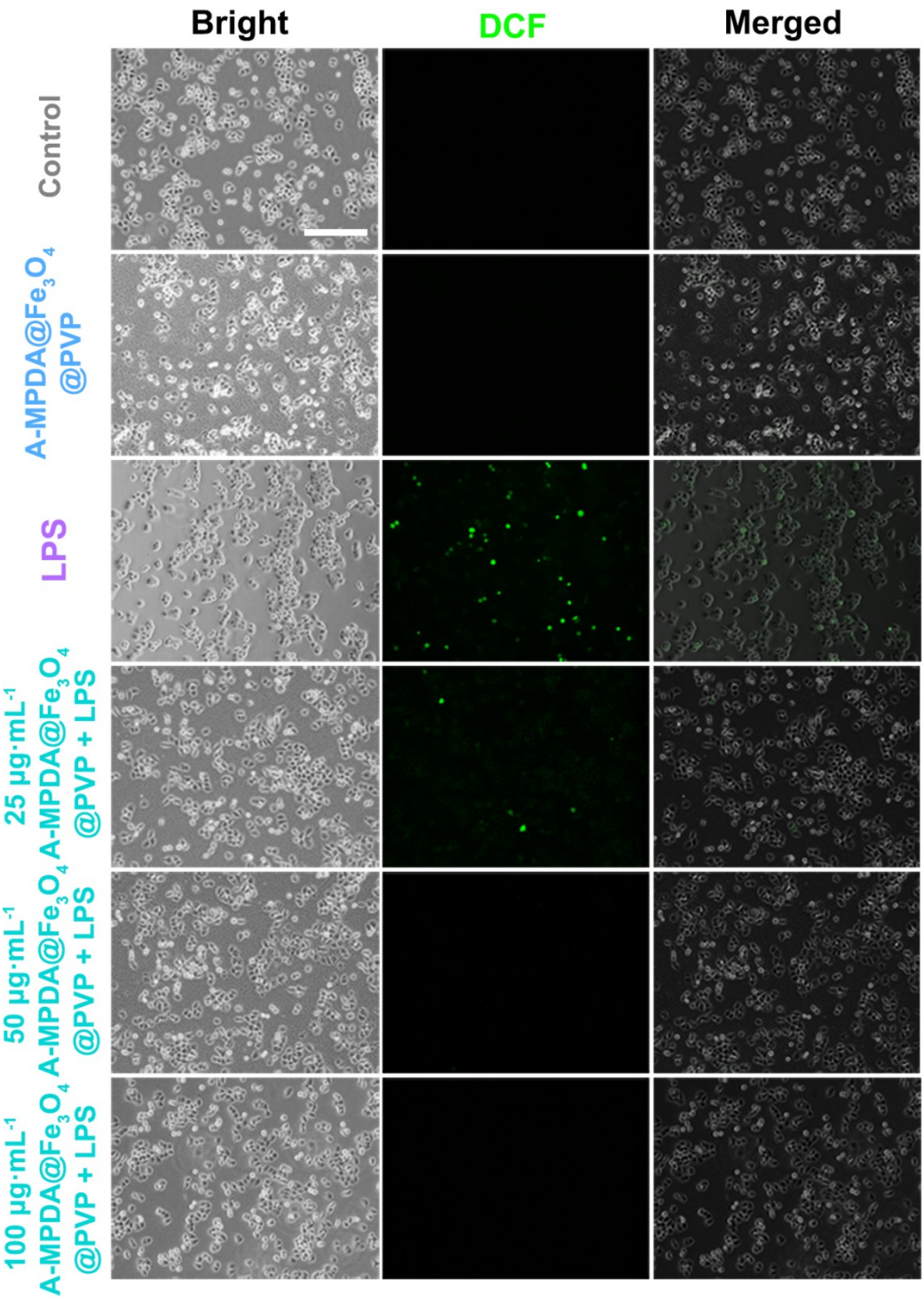

Fig. S8. Representative intracellular ROS staining of untreated and different concentration of A-MPDA@Fe_3O_4@PVP NPs-treated L02 cells with LPS treatment (20 μg·mL^{-1}). Scale bar: 300 μm.

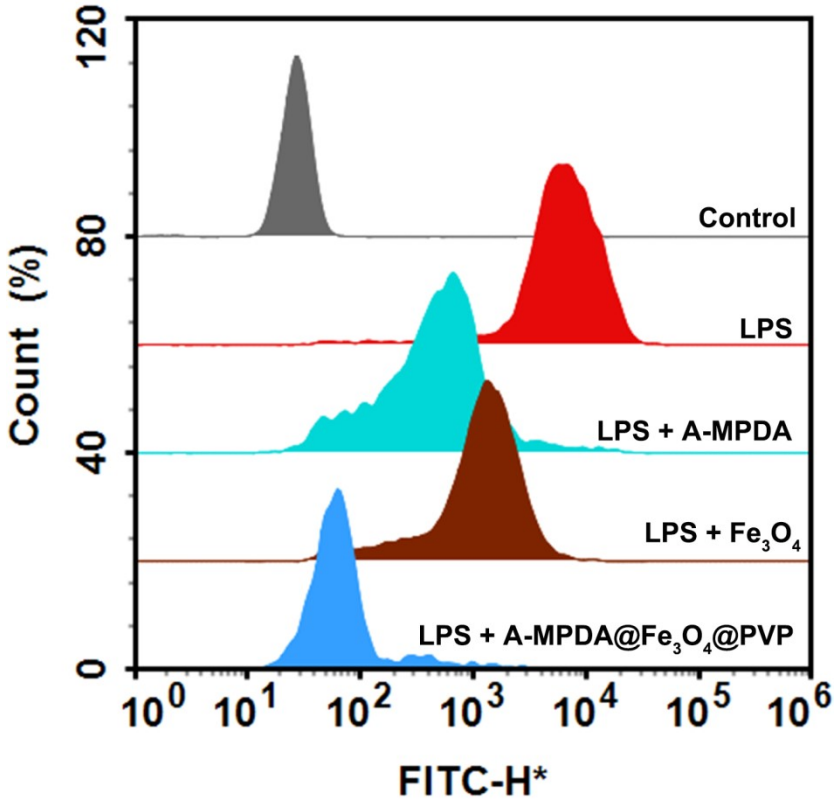

Fig. S9. Flow cytometry analysis of representative intracellular ROS staining of different nanoparticles -treated cells with LPS treatment.

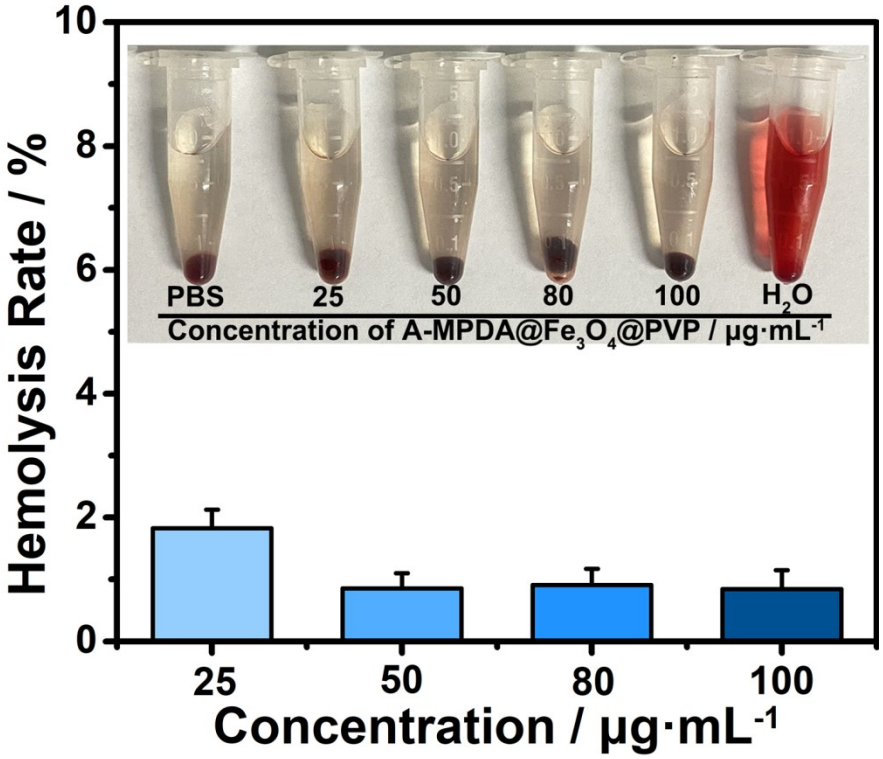

Fig. S10. Hemolytic assays of A-MPDA@Fe_3O_4@PVP NPs in different concentration.

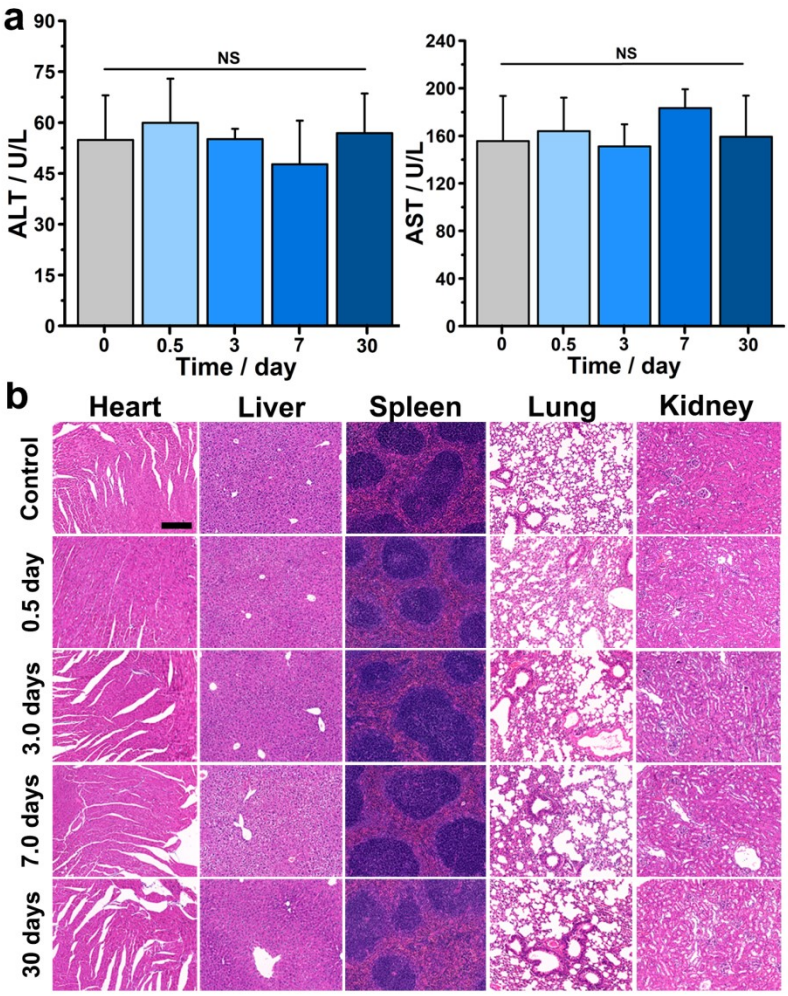

Fig. S11 *In vivo* biocompatibility of A-MPDA@Fe_3O_4@PVP NPs. (a) Serum levels as part ALT, AST. *n*=5 per group; (b) Representative H&E staining images of the main organs at 0.5, 3, 7, and 30 days after intravenous injection of 5 mg·kg^{-1} A-MPDA@Fe_3O_4@PVP NPs on healthy mice. Scale bar: 200 μm

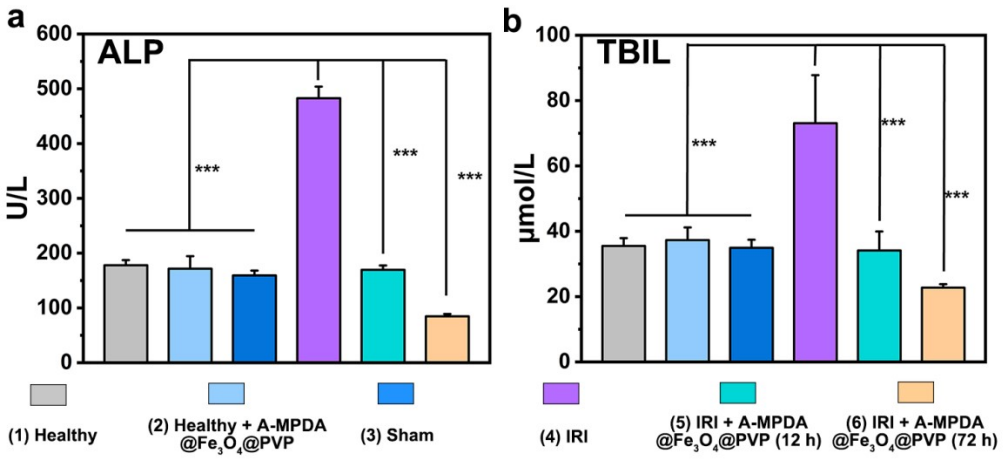

Fig. S12. Change in serum ALP a) and TBIL b) levels from various groups of mice (n = 4).